Article

Quenching Stress of Hot-Rolled Seamless Steel Tubes under Different Cooling Intensities Based on Simulation

Zhenlei Li [1], Rui Zhang [1], Dong Chen [1], Qian Xie [2],*, Jian Kang [1], Guo Yuan [1],* and Guodong Wang [1]

1   State Key Laboratory of Rolling and Automation, Northeastern University, Shenyang 110819, China
2   School of Metallurgic Engineering, Anhui University of Technology, Ma'anshan 243002, China
*   Correspondence: xieqian@ahut.edu.cn (Q.X.); yuanguoneu@163.com (G.Y.)

Abstract: Large residual stress occurs during the quenching process of hot-rolled seamless steel tubes, which results in bending, cracking, and ellipticity exceeding standards and seriously affects the quality of hot-rolled seamless steel tubes. In addition, the stress generation mechanism of hot-rolled seamless steel tubes is different from that of steel plates due to the characteristics of annular section. In this research, the finite element simulation method was used to study the quenching residual stress of seamless steel tubes with different cooling intensities. The variation law of temperature and stress on the steel tube under different cooling intensities were analyzed. The results show that the radial stress was close to 0, and the circumferential and axial stresses were the main factors affecting the quality of the steel tube. With the increase in the cooling time, the magnitude and direction of each stress component of the steel tube changed simultaneously. Finally, a typical stress distribution state of "external compressive stress, internal tensile stress" was presented in the thickness direction of the steel tube. Furthermore, with the increase in the cooling intensity, the residual stress of the steel tube gradually increased and was mainly concentrated on the near wall of the steel tube.

Keywords: seamless steel tubes; residual stress; finite element simulation; heat transfer coefficient; cooling intensity

1. Introduction

As an important steel variety, hot-rolled seamless steel tubes are widely used in energy extraction, petrochemical and machinery manufacturing, and other fields [1–3]. With the acceleration of economic construction and the increasingly complex environment for energy extraction, such as oil and natural gas, higher performance requirements must be met by hot-rolled seamless steel tubes. As one of the important links in the production process of metal materials, the heat treatment process can fully tap the potential of the material, increase intensity, and improve the plasticity and welding performance [4]. However, during the quenching process of hot-rolled seamless steel tubes, due to the cooling difference between the inner and outer walls, there is a large temperature gradient in thickness, which leads to internal thermal stress. When the stress exceeds the yield intensity of the steel tube, problems occur, such as bending, cracking, or ellipticity changes, which seriously affect product quality [5,6]. In addition, the distribution of residual stress is greatly related to the shape. Compared with the plates, the characteristics of the annular hollow section of hot-rolled seamless steel tubes make the stress generation mechanism more complicated, which greatly increases the difficulty of residual stress analysis. Thus, the research progress in quenching stress in the field of steel tubes is far behind that of steel plates. It is important to study the generation mechanism and evolution law of stress in the quenching process of hot-rolled seamless steel tubes, which greatly contribute to the improvement in the quality of hot-rolled seamless steel tubes.

Previous studies mainly focused on the heat transfer of steel tubes or cylindrical surfaces [7–11], but stress changes during cooling were rarely reported. Ali et al. [12] studied

the comprehensive effects of time, material properties, and the ratio of the inner and outer radius on the transient temperature gradient and provided an empirical solution for the thermal stress of the cylinder under the conditions of heating, secondary heating, and forced-air impact cooling. Schemmel et al. [13] investigated the formation of residual stress and the evolution of phase components during the quenching process of cylindrical specimens with different sizes. They found that the surface residual stress changed from tensile stress to compressive stress when the size of the steel tube was increased. Hata et al. [14] theoretically analyzed the thermal stress induced by thermal shock and the stress-focusing effect induced by phase transformation stress. They pointed out that, in the quenched state, cracks may occur in the center of the cylindrical rod due to the interaction of the thermal phase transition stress-focusing effect and the phase transition stress-focusing effect. Oliveira et al. [15] showed the thermodynamic behavior of a cylinder and established a non-isothermal multiphase constitutive equation. Chen et al. [16] carried out related research on the problem of axial cracks caused by thermal shock in coated hollow cylinders; they used the finite element method to calculate the transient temperature and induced the thermal stress and crack tip stress intensity factors of the inner surface of the cylinder after convective cooling. Devynck et al. [17] studied the effect of boiling heat transfer and phase transformation on the quenching deformation of steel tubes by simulation and experimentation. Their calculated results regarding the bending of the steel tube corresponded to the measured values. Leitner et al. [18] used finite element simulation and experimentation to study how to use a controlled cooling strategy to control residual stress and phase structure in multiphase steel tubes, and pointed out that using a low cooling rate would result in a lower plasticity and residual stress. Yang et al. [19] also used the finite element method to study the effects of quenching water temperature, the rod length-to-diameter ratio, pre-stretching ratio, and stretching rate on the residual stress of quenched rods after cold stretching. They showed that the maximum residual tensile and compressive stress of the quenched rod decreases with the increase in the water temperature.

The magnitude of residual stress of hot-rolled seamless steel tubes depends on the cooling intensity during the quenching process. At present, the cooling intensity control of steel tubes can be realized by changing the water flow and temperature of the cooling medium [20]. In this paper, relevant research was carried out on the variation law of temperature and stress during the quenching process of hot-rolled seamless steel tubes under different cooling intensities. The purpose was to explore the inherent laws of cooling intensity, temperature field, and stress field and to provide data support and theoretical reference for the design of a heat treatment process for eliminating the residual stress of seamless steel tubes.

2. FEM Model of Quenching Process

2.1. Materials and Methods

As shown in Figure 1, the heat treatment process of materials is a complex process of chemical composition, temperature field, metallurgy field, and stress field coupling [21–24]. The metal workpiece after heat treatment can undergo a solid-phase transformation when the temperature changes in the solid-state range. Different phases can be obtained by controlling the progress of the solid-state-phase transition. There are differences in the stacking ratio and specific heat capacity of different phases. During the cooling process of the workpiece, due to the existence of the temperature gradient in the workpiece cross-section, the phase transformation of the workpiece cannot be carried out at the same time. This internal stress due to phase-transition asynchrony is called microstructure stress, and the resulting strain is called microstructure strain. It is difficult to obtain the real-time changing state of stress and predict the residual stress field. Thus, it is difficult to carry out targeted prevention and elimination measures. As a finite element simulation software, ANSYS can handle any material, any complex shape, any boundary, and any time or heat treatment process, which can shorten the research time and lower the research and

development costs. Therefore, this paper used ANSYS software to simulate the temperature field and stress field of hot-rolled seamless steel tubes under different cooling intensities.
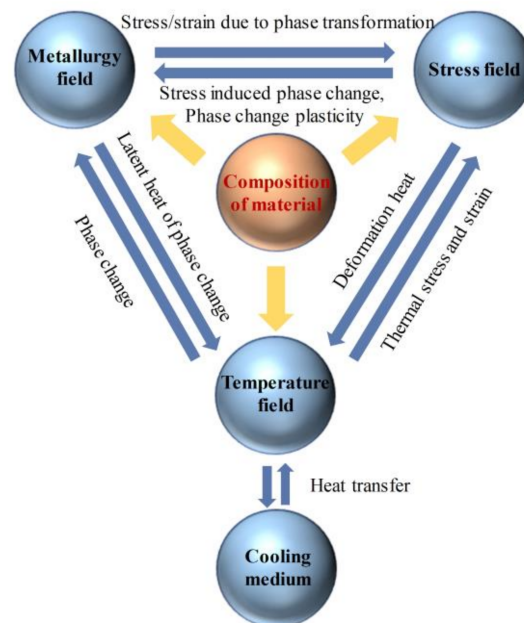

Figure 1. Multiphysics and coupling interactions involved in heat treatment engineering.

The size of the steel tube was $140 \times 20 \times 400$ mm. Because the steel tube was an axisymmetric model, the 1/8 model was selected for simulation in order to reduce the simulation time, as shown in Figure 2. The material of the steel tube that was to be heat-treated was 310S stainless steel, which experiences no phase transformation process during heat treatment. Thus, the research problem was simplified to the interaction between the temperature field and the stress field. The thermophysical parameters of 310S stainless steel were determined through linear interpolation, as shown in Figure 3.
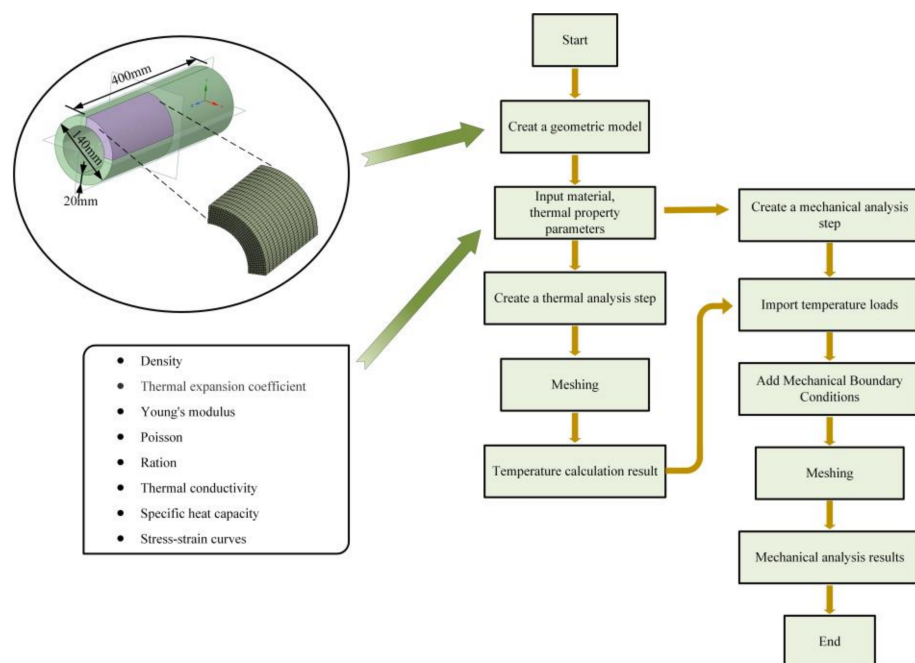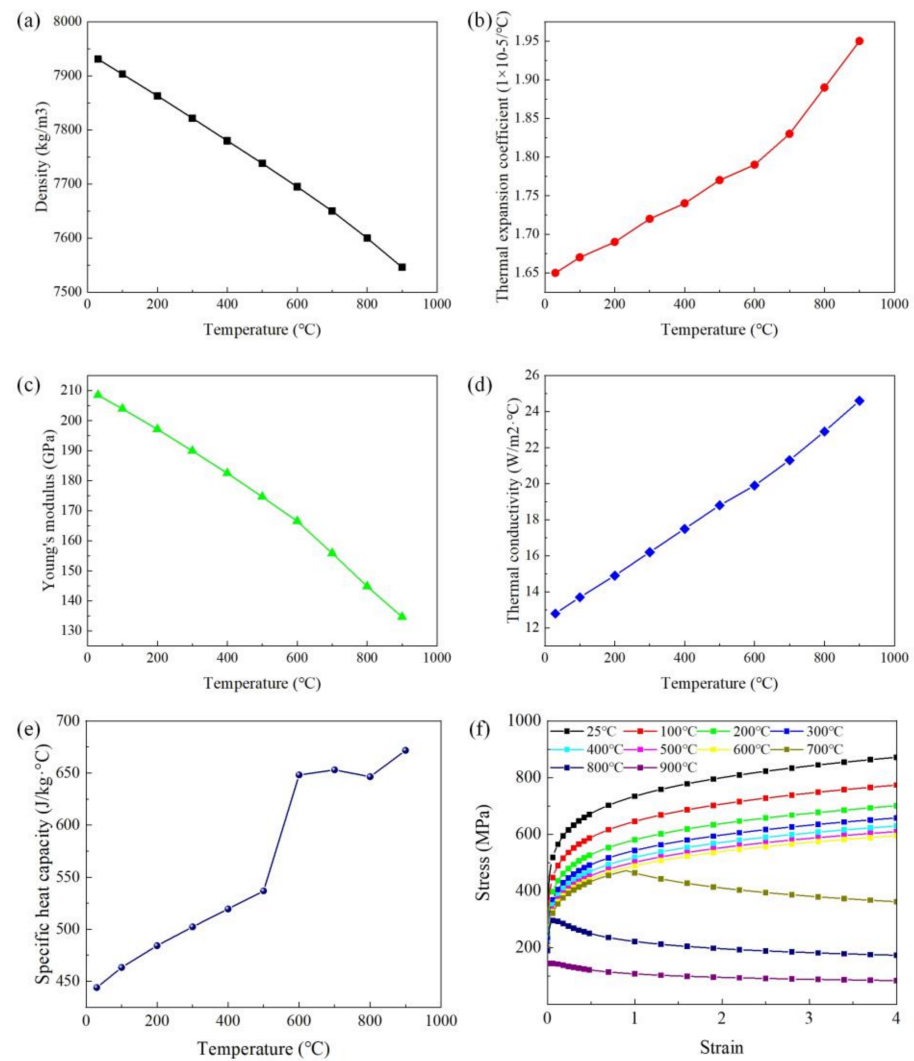

Figure 2. Finite element model and calculation process.

Figure 3. The thermophysical parameters of 310S stainless steel. (**a**) desnity; (**b**) thermal expansion cofficient; (**c**) Young's modulus; (**d**) thermal conducivity; (**e**) specific heat capacity; (**f**) stress−strain curves.

2.2. Mathematical Model

The calculation of the temperature field is achieved using the three-dimensional thermal conductivity differential equation in the cylindrical coordinate system, and its expression is shown as follows [7,10,25]:

$$\frac{1}{r}\frac{\partial}{\partial r}\left(\lambda r\frac{\partial T}{\partial r}\right) + \frac{1}{r^2}\frac{\partial}{\partial \varphi}\left(\lambda\frac{\partial T}{\partial \varphi}\right) + \frac{\partial}{\partial z}\left(\lambda\frac{\partial T}{\partial z}\right) + \dot{\Phi} = \rho c\frac{\partial T}{\partial t} \tag{1}$$

where λ is the thermal conductivity; ρ is the material density; c is the material-specific heat capacity; T is the temperature of the steel tube; t is the time; r is the radial distance of the steel tube; φ is the azimuth angle; z is the height; and $\dot{\Phi}$ is the internal heat source, which comes from the heat released by the phase transition during the quenching process, and because there is no phase transition in this simulation, the value is 0.

In order to determine the unique thermal conductivity differential equation, the initial and boundary conditions need to be given. The initial condition refers to the temperature distribution (T_0) of the object area at the initial time, which is expressed by Equation (2):

$$T|_{t=0} = T_0 \tag{2}$$

The third type of boundary condition is used to set the temperature of the cooling medium and the surface heat transfer coefficient during the quenching process of the steel tube, and its expression is shown as follows:

$$- \lambda \left(\frac{\partial T}{\partial n} \right) = h \left(T_w - T_f \right) \tag{3}$$

In this finite element simulation, the initial temperature of the steel tube (T_w) is 900 °C, the cooling water temperature (T_f) is 30 °C. Using the single-variable method, only the cooling intensity of the single wall is changed each time. When the heat transfer coefficient of the inner wall (h_{inner}) is 600 W/(m^2·°C), the heat transfer coefficient of the outer wall (h_{outer}) is set to four control groups: 1000, 2000, 3000, and 4000 W/(m^2·°C). Similarly, when the heat transfer coefficient of the outer wall (h_{outer}) is 1000 W/(m^2·°C), the heat transfer coefficient of the outer wall (h_{inner}) is set to four control groups: 200, 600, 1000, and 1400 W/(m^2·°C). Since the cooling intensity of inner wall is lower than that of outer wall in actual production, the heat transfer coefficient of the inner wall is smaller than that of the outer wall.

For the linear elastic model, the incremental relationship between stress and strain is expressed in Equation (4).

$$d\sigma = D_e d\varepsilon \tag{4}$$

$$D_e = \frac{E}{(1+v)(1-2v)} \begin{bmatrix} 1-v & v & v & 0 & 0 & 0 \\ v & 1-v & v & 0 & 0 & 0 \\ v & v & 1-v & 0 & 0 & 0 \\ 0 & 0 & 0 & \frac{1-2v}{2} & 0 & 0 \\ 0 & 0 & 0 & 0 & \frac{1-2v}{2} & 0 \\ 0 & 0 & 0 & 0 & 0 & \frac{1-2v}{2} \end{bmatrix} \tag{5}$$

where $d\sigma$ is the stress increment, $d\varepsilon$ is the strain increment, D_e is the elastic modulus matrix, E is the elastic modulus, and v is the Poisson ratio.

Because stainless steel is used in this simulation, there is no phase transition, and the phase transition strain increment is 0. For the thermo-elastoplastic model for calculating thermal stress, the strain increment is expressed by Equation (6).

$$d\varepsilon = d\varepsilon_e + d\varepsilon_p + d\varepsilon_T \tag{6}$$

where $d\varepsilon_e$, $d\varepsilon_p$, and $d\varepsilon_T$ are the elastic strain increment, the plastic strain increment, and the thermal strain increment.

$$d\varepsilon_e = \frac{1}{2G} d\sigma' + \frac{1-2v}{E} d\sigma_m \delta_{ij} \tag{7}$$

where $d\sigma'$ and $d\sigma_m$ are the stress deviator increment and mean stress increment.

The shear modulus G is shown in the following equation:

$$G = \frac{E}{2(1+v)} \tag{8}$$

The Kronecker symbol is defined as follows:

$$\delta_{ij} = \begin{cases} 1, & i = j \\ 0, & i \neq j \end{cases} \tag{9}$$

The flow criterion is an assumption that indicates the direction of the plastic deformation increment after the material reaches yield, that is, a proportional relationship between

the components of the plastic deformation increment. The plastic strain increment is shown in the following equation:

$$d\varepsilon_p = d\lambda\sigma' = \frac{3}{2}\frac{d\overline{\varepsilon_p}}{\sigma}\sigma' \tag{10}$$

where $d\lambda$, σ', $d\overline{\varepsilon_p}$, and σ are the instantaneous scaling factor, the stress deviator, the equivalent plastic strain increment, and the equivalent stress.

The thermal strain increment can be expressed as:

$$d\varepsilon_T = \sum_{k=1}^{n} y_k \alpha_k dT \tag{11}$$

In the formula, y_k refers to the volume fraction of the phase k in the material; n refers to number of phases in the material; and α_k refers to the thermal expansion coefficient of the phase k related to the temperature. Since 310S stainless steel is used in this paper, only the austenite phase exists, so the thermal strain increment formula can be simplified as:

$$d\varepsilon_T = \alpha dT \tag{12}$$

2.3. Verification of Other Finite Element Simulation Cases

In order to verify the accuracy of the residual stress simulation, the finite element simulation results are compared with the experimental data in reference [26]. Reference [26] studied the quenching residual stress distribution of 7050 Al ingot by means of experiments and finite element simulation. Because the ingot is a symmetrical model, in order to reduce the calculation time, only a quarter of the model is used in this simulation. As shown in Figure 4, the simulation data gathered in this paper are compared with the residual stress in reference [26]. It can be seen from the figure that although a certain error occur in the simulated data compared to the experimental data, the same trend is maintained.
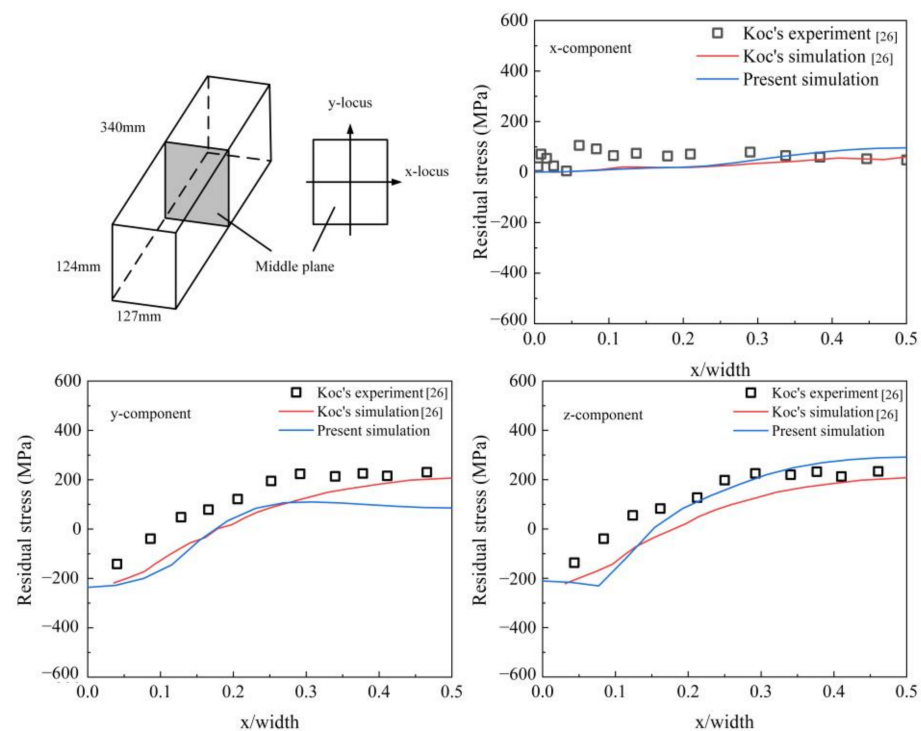

Figure 4. Comparison of the simulated data and experimental data [26].
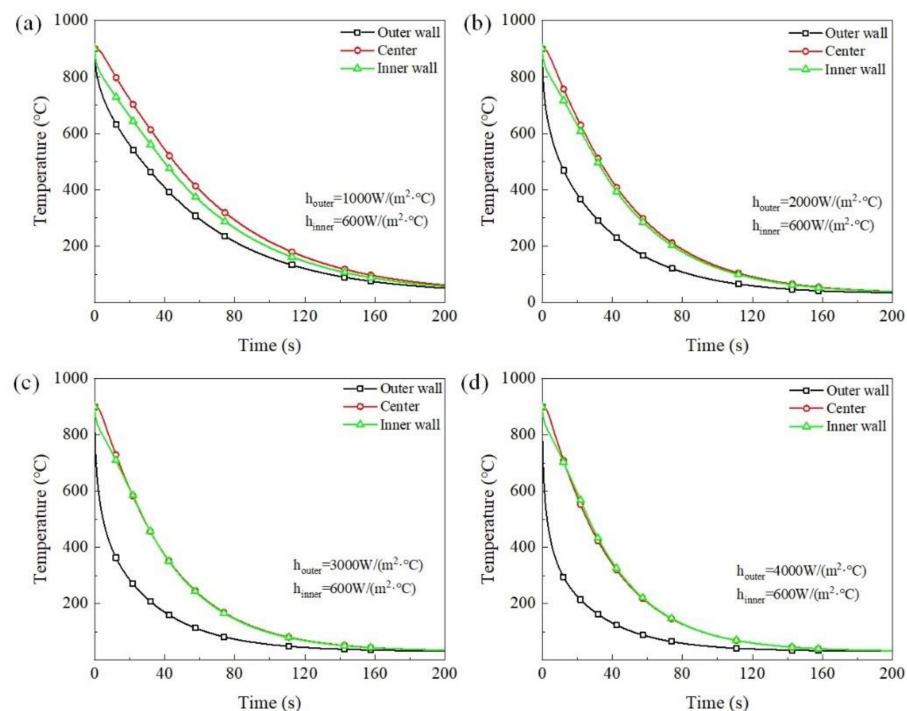
3. Results and Discussion

3.1. Different Cooling Intensities of the Outer Wall

Figure 5 shows the temperature curves of the steel tube under different cooling intensities of the outer wall. It can be seen from Equation (3) that the heat transfer was related to the temperature gradient. At the initial moment, the temperature of the steel tube was high, there was a large temperature gradient within the surrounding environment, the heat transfer rate was fast, and the temperature dropped rapidly. Then, as the cooling time increased, the temperature of the steel tube gradually decreased. The gradient, with respect to the ambient temperature, gradually decreased, and the decreasing trend of the temperature gradually slowed down. Eventually, the steel tube cooled to ambient temperature with zero heat transfer. By comparison, it was found that with the increase in the convection heat transfer coefficient of the outer wall, the temperature of the outer wall decreased faster. Figure 6 shows the temperature distribution cloud map of the steel tube.

Figure 7 shows the equivalent stress under different cooling intensities of the outer wall. The von Mises criterion was adopted as the effective stress. It was calculated by Equation (13). There was no sign of the calculation result, so the state of stress could not be judged.

$$(\sigma_r - \sigma_\theta)^2 + (\sigma_\theta - \sigma_z)^2 + (\sigma_z - \sigma_r)^2 = 2\sigma_s^2 \tag{13}$$

The maximum equivalent stress was 341.99 MPa when h_{outer} = 1000 W/(m$^2\cdot°$C), as shown in Figure 7a. When h_{outer} = 2000 W/(m$^2\cdot°$C), the maximum equivalent stress was 397.42 MPa and increased by 55.43 MPa. When h_{outer} = 3000 W/(m$^2\cdot°$C), the maximum equivalent stress was 428.01 MPa and increased by 30.59 MPa. When h_{outer} = 4000 W/(m$^2\cdot°$C), the maximum equivalent stress was 447.69 MP and increased by 19.68 MPa. The maximum equivalent stress was mainly concentrated on the outer wall. With the increase in the cooling intensity, the maximum equivalent stress of the steel tube gradually increased, but the increase trend gradually slowed down.

Figure 5. Temperature curves of the steel tube at different cooling intensities of the outer wall. (**a**) h_{outer} = 1000 W/(m$^2\cdot°$C); (**b**) h_{outer} = 2000 W/(m$^2\cdot°$C); (**c**) h_{outer} = 3000 W/(m$^2\cdot°$C); (**d**) h_{outer} = 4000 W/(m$^2\cdot°$C).
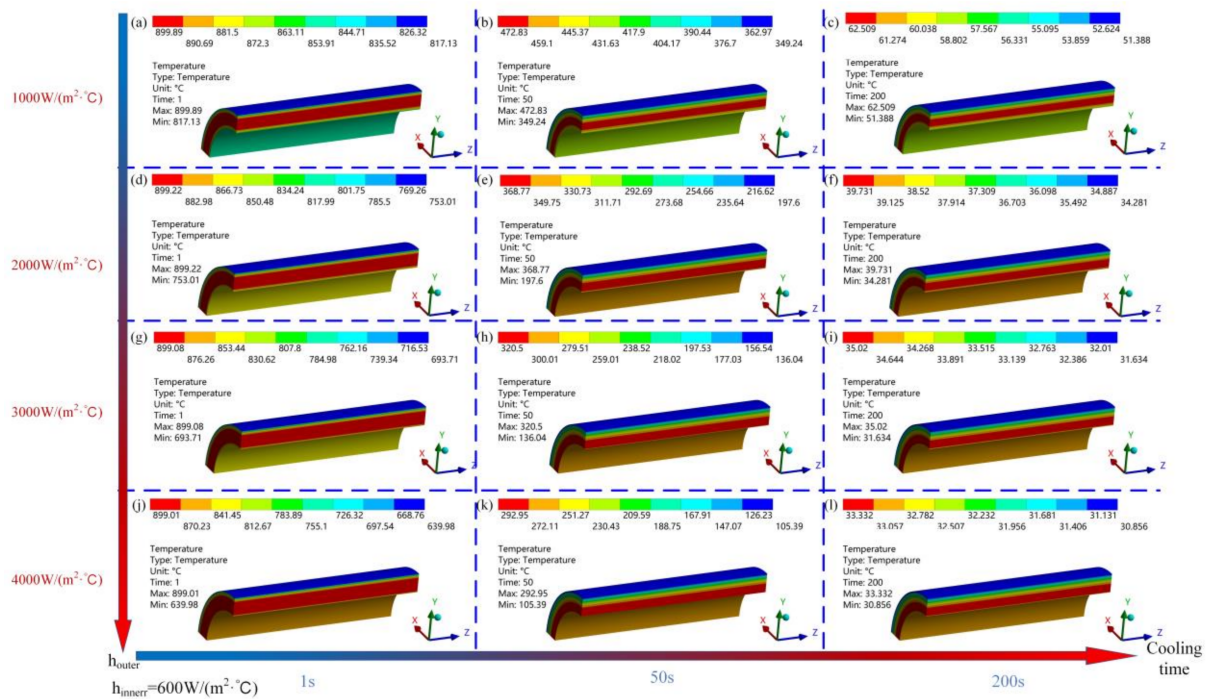
Figure 6. The temperature fields' evolution in the quenching process of the steel tube under different cooling intensities of the outer wall. (**a**) h_{outer} = 1000 W/(m²·°C), t = 1 s; (**b**) h_{outer} = 1000 W/(m²·°C), t = 50 s; (**c**) h_{outer} = 1000 W/(m²·°C), t = 200 s; (**d**) h_{outer} = 2000 W/(m²·°C), t = 1 s; (**e**) h_{outer} = 2000 W/(m²·°C), t = 50 s; (**f**) h_{outer} = 2000 W/(m²·°C), t = 200 s; (**g**) h_{outer} = 3000 W/(m²·°C), t = 1 s; (**h**) h_{outer} = 3000 W/(m²·°C), t = 50 s; (**i**) h_{outer} = 3000 W/(m²·°C), t = 200 s; (**j**) h_{outer} = 4000 W/(m²·°C), t = 1 s; (**k**) h_{outer} = 4000 W/(m²·°C), t = 50 s; (**l**) h_{outer} = 4000 W/(m²·°C), t = 200 s.
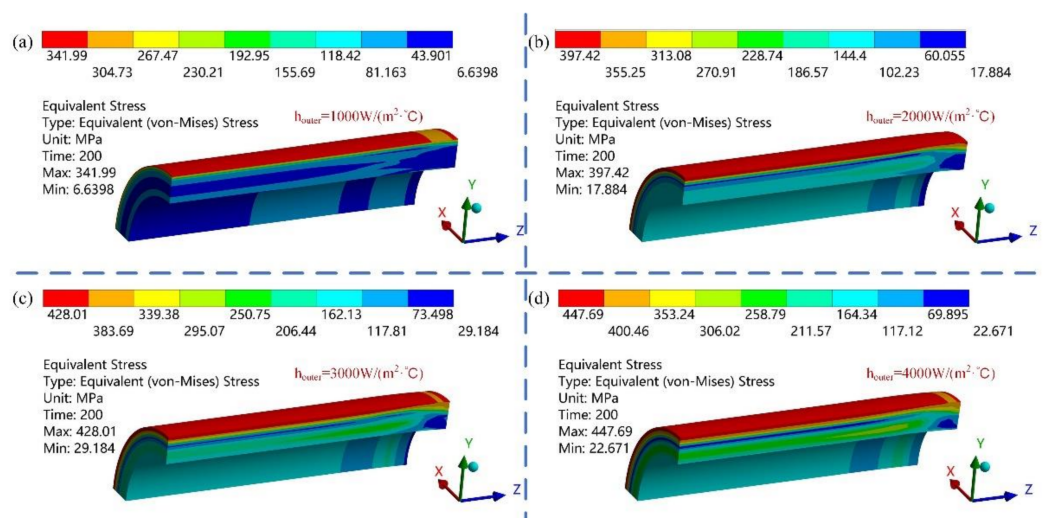
Figure 7. Distribution of the equivalent stress filed at different cooling intensities of the outer wall. (**a**) h_{outer} = 1000 W/(m²·°C); (**b**) h_{outer} = 2000 W/(m²·°C); (**c**) h_{outer} = 3000 W/(m²·°C); (**d**) h_{outer} = 4000 W/(m²·°C).

Figure 8 shows the variation curves of the radial stress, circumferential stress, and axial stress with the time at different positions. As can be seen from Figure 8, the radial stress (σ_r) was close to 0, which was much smaller than the circumferential (σ_θ) and axial stress (σ_z). The circumferential and axial stresses were the main factors affecting the quality

of the steel tube during the quenching process. With the increase in the cooling intensity of the outer wall, the stress components of the steel tube increased. In the early stage of cooling of the steel tube, the outer wall rapidly cooled, forming a large temperature gradient with the inside and shrinking to the inside. Each stress component reached its peak in a short time. With the increase in the cooling time, each stress component gradually decreased and the direction changed.
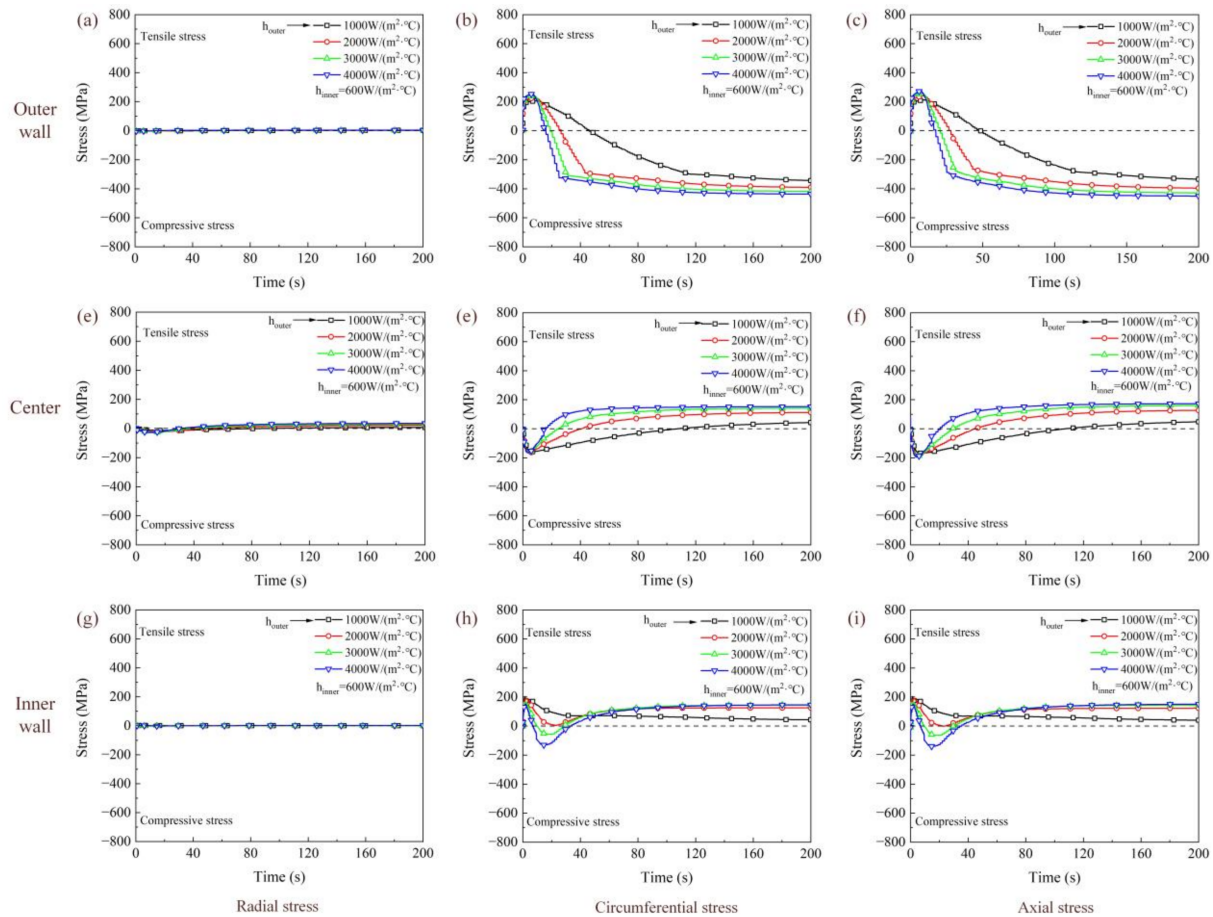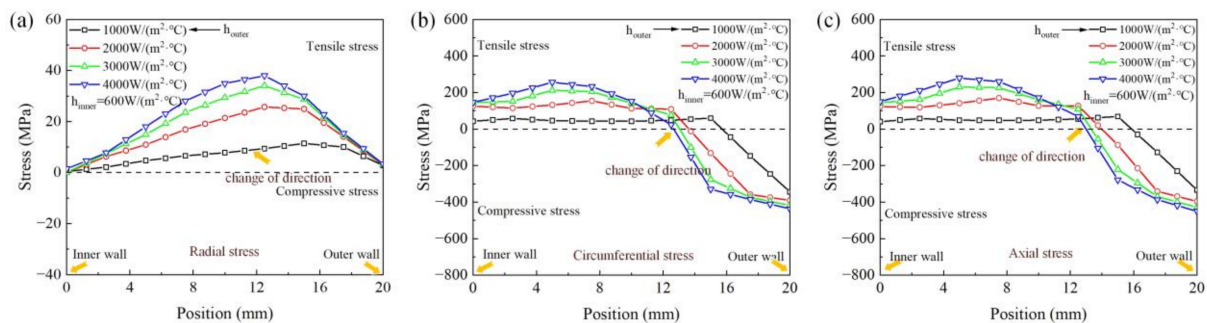

Figure 8. Stress-time curves of different positions under different cooling intensities of the outer wall. (**a**) radial stress of the outer wall; (**b**) circumferential stress of the outer wall; (**c**) axial stress of the outer wall; (**d**) radial stress of the center; (**e**) circumferential stress of the center; (**f**) axial stress of the center; (**g**) radial stress of the inner wall; (**h**) circumferential stress of the inner wall; (**i**) axial stress of the inner wall.

As shown in Figure 8b,c, the outer wall of the steel tube was restricted by the internal material, which hindered the further development of its shrinkage. The outer wall was subjected to tensile stress in the circumferential and axial directions. As the temperature of the outer wall further decreased, the cooling rate of the outer wall was lower than the cooling rate of the center, so that the shrinkage of the center was greater than that of the outer wall, and the stress on the outer wall gradually decreased. When the steel tube was cooled to a certain temperature, the direction of the stress changed. The outer wall was subjected to compressive stress in the circumferential and axial directions. On the contrary, as shown in Figure 8e,f, the center was subjected to pressure from the outer wall at the initial stage; as the cooling rate of the outer wall gradually decreased, the compressive stress on the center gradually decreased, and the direction of the stress finally changed and became tensile stress.

It can be seen from Figure 8h,i that the direction of the stress on the inner wall changed twice. This was due to a shift in the magnitude relationship between the cooling rates of the

outer wall, the center, and the inner wall. As shown in Figure 8, in the initial cooling stage, the cooling rate of the inner wall of the steel tube was greater than the heat conduction of the wall, and the inner wall surface shrank, so the inner wall was subjected to the tensile stress exerted by the center in the circumferential and axial directions. While the cooling time increased, the cooling rate of the center was greater than that of the inner wall. The tensile stress on the inner wall gradually decreased, and the direction of the stress changed. When the cooling rate of both the inner wall and the center was greater than that of the outer wall surface, the direction of stress changed again and the inner wall was subjected to the tensile stress exerted by the outer wall.

In the radial direction, there was tensile stress at the center, and the maximum stress appeared near the outer wall, while the stress near the inner and outer walls was close to 0, as seen in Figure 9. In the axial direction, there was compressive stress on the surface and tensile stress at the center, and the maximum stress appeared on the outer wall of the steel tube. The distribution of the circumferential stress was similar to that of the axial stress. The magnitude of the residual stress increased with the increase in the cooling intensity, and the position where the stress direction changed gradually moved to the center, with an increase in the cooling intensity on the outer wall.


Figure 9. Stress distribution curve under different cooling intensities of the outer wall. (**a**) radial stress; (**b**) circumferential stress; (**c**) axial stress.

3.2. Different Cooling Intensities of the Inner Wall

With the increase in the cooling intensity of the inner wall, the cooling rate gradually increased, and the temperature curves of the inner and outer walls gradually tended to be consistent (as is shown in Figure 10). When the cooling intensity of the inner and outer walls were the same, the cooling rate of the inner wall was smaller than the cooling rate of the outer wall. This is because the heat transfer area gradually increased from the inside to the outside during the cooling process of the steel tube. On the contrary, the heat transfer area gradually decreased from the outside to the inside. Figure 11 shows the cloud map of the temperature distribution under different cooling intensities of the inner wall. As the cooling intensity of the inner wall increased, the position of the highest temperature gradually moved to the center of the steel tube.
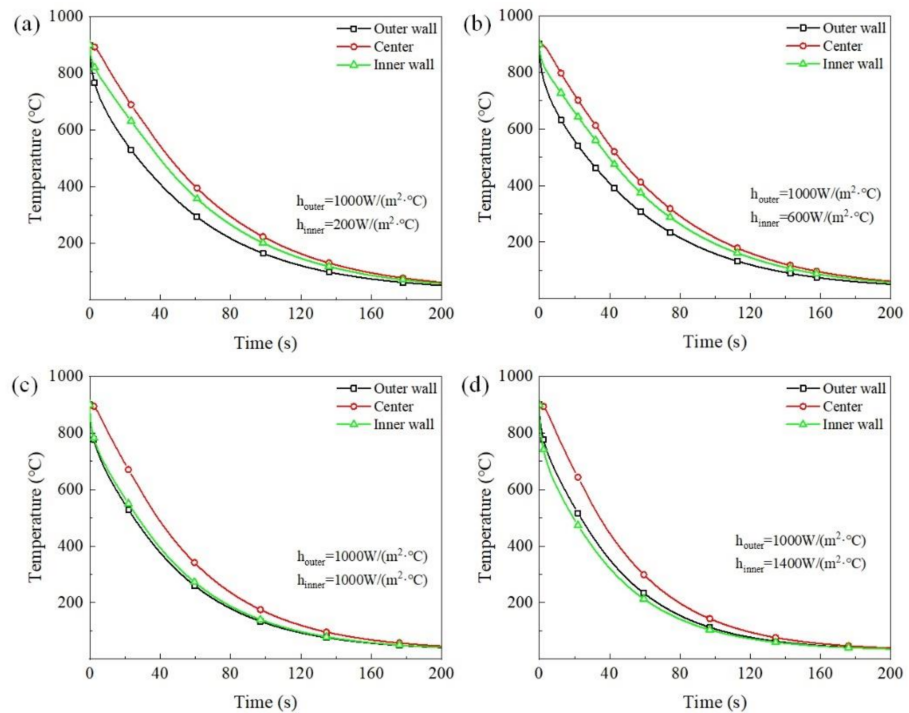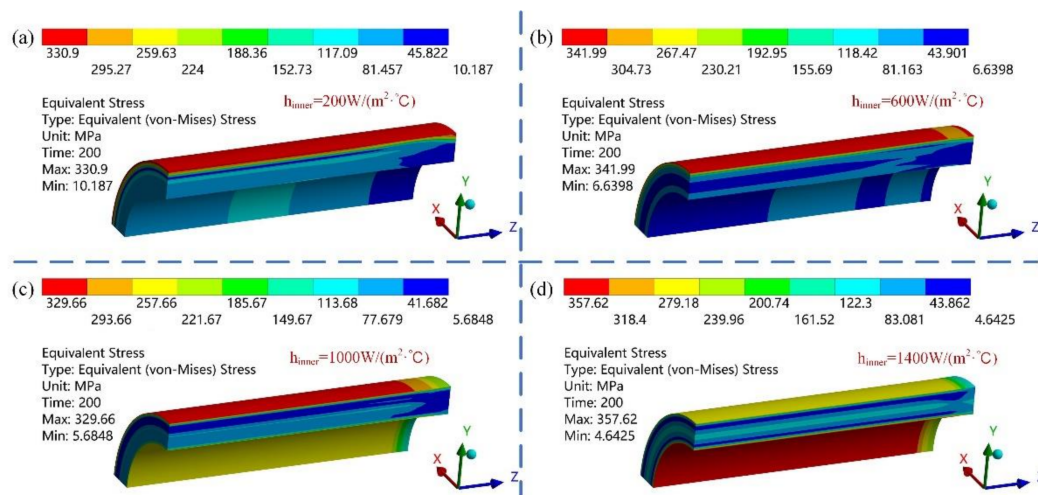
Figure 10. Temperature curves of the steel tube under different cooling intensities of the inner wall. (**a**) h_{inner} = 200 W/(m²·°C); (**b**) h_{inner} = 600 W/(m²·°C); (**c**) h_{inner} = 1000 W/(m²·°C); (**d**) h_{inner} =1400 W/(m²·°C).
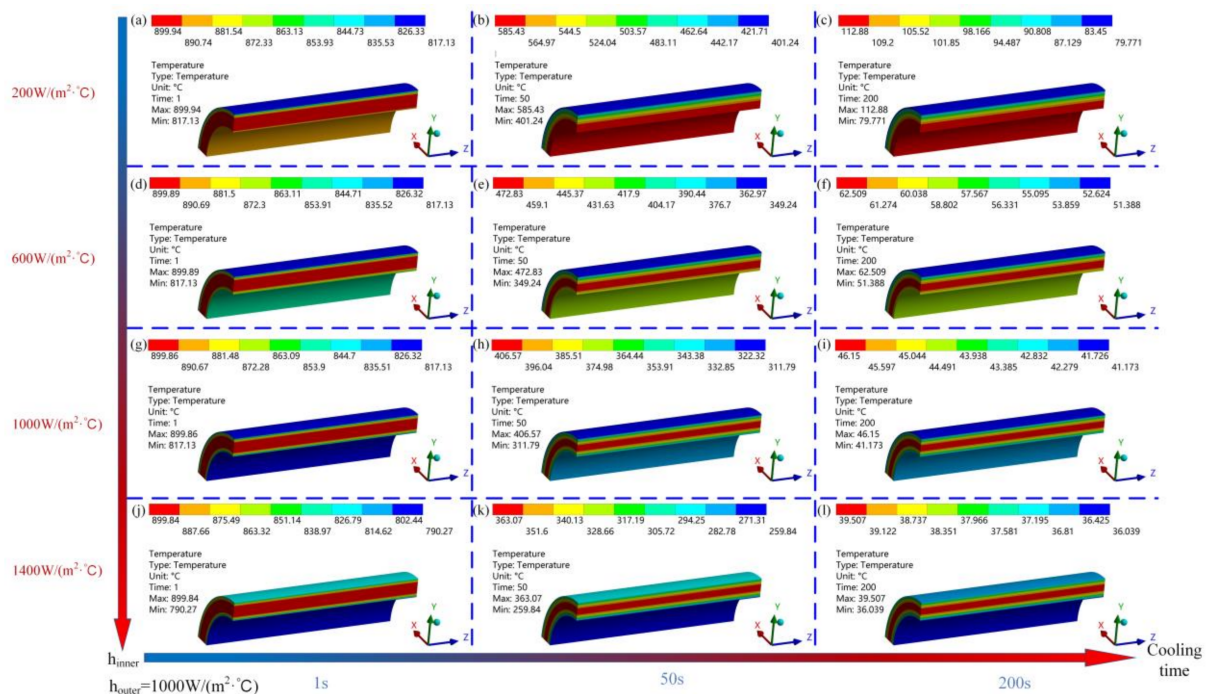
Figure 11. The temperature fields' evolution in the quenching process of the steel tube under different cooling intensities of the inner wall. (**a**) h_{inner} = 200 W/(m²·°C), t = 1 s; (**b**) h_{inner} = 200 W/(m²·°C), t = 50 s; (**c**) h_{inner} = 200 W/(m²·°C), t = 200 s; (**d**) h_{inner} = 600 W/(m²·°C), t = 1 s; (**e**) h_{inner} = 600 W/(m²·°C), t = 50 s; (**f**) h_{inner} = 600 W/(m²·°C), t = 200 s; (**g**) h_{inner} = 1000 W/(m²·°C), t = 1 s; (**h**) h_{inner} = 1000 W/(m²·°C), t = 50 s; (**i**) h_{inner} = 1000 W/(m²·°C), t = 200 s; (**j**) h_{inner} = 1400 W/(m²·°C), t = 1 s; (**k**) h_{inner} = 1400 W/(m²·°C), t = 50 s; (**l**) h_{inner} = 1400 W/(m²·°C), t = 200 s.

Figure 12 shows the cloud diagram of the equivalent stress at different cooling intensities of the inner wall. When the cooling intensity of the inner wall was small, the maximum equivalent stress was mainly concentrated on the outer wall. However, when the cooling intensity of the inner wall was greater than the cooling intensity of the outer wall, the maximum equivalent stress was located on the inner wall. With the increase in the cooling intensity of the inner wall, the maximum equivalent stress first decreased and then increased.


Figure 12. Distribution of the equivalent stress field at different cooling intensities of the inner wall. (**a**) h_{inner} = 200 W/(m^2·°C); (**b**) h_{inner} = 600 W/(m^2·°C); (**c**) h_{inner} = 1000 W/(m^2·°C); (**d**) h_{inner} = 1400 W/(m^2·°C).

The initial moment of circumferential and axial stresses on the outer wall was tensile stress, as shown in Figure 13. With the increase in the cooling time, the stress state changed to compressive stress. The stress at the center changed from compressive stress to tensile stress. This was similar to the change law of stress when changing the cooling intensity of the outer wall. It is worth noting that when the cooling intensity of the inner wall was 200 W/(m^2·°C), although the initial stress in the circumferential and axial directions was tensile stress, it transformed into compressive stress in a short period of time, and transformed into tensile stress with the increasing cooling time. As the cooling intensity of the inner wall increased, the circumferential and axial stresses of the inner wall only changed the direction of the stress once, from tensile stress to compressive stress.

Figure 14 shows the distribution of residual stress in the direction of the steel tube at different inner wall cooling intensities. When the cooling intensity of the inner wall was less than that of the outer wall, all the radial stresses were tensile stress. When the cooling intensity of the inner wall was greater than that of the outer wall, the stress of the near outer wall was tensile stress and the stress of the near inner wall was compressive stress. With the increase in the cooling intensity, the circumferential and axial stress changed from tensile stress to compressive stress, and the position of transformation moved gradually closer to the center. The position where the tensile stress changed from compressive stress was close to the outer wall, which was contrary to the changing trend of the cooling intensity of the outer wall, as seen in Figure 9.
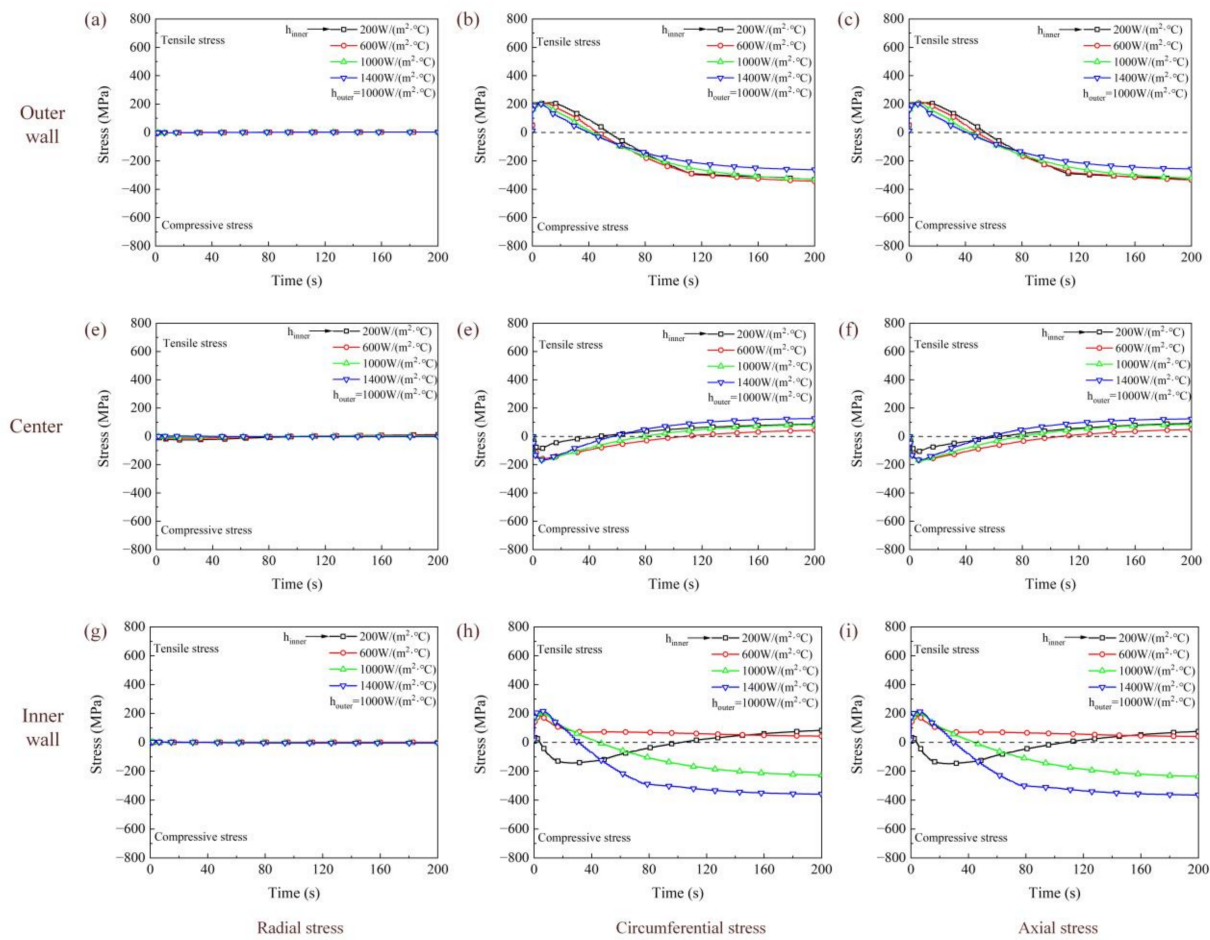
Figure 13. Stress-time curves of different positions with time at different cooling intensities of the inner wall. (**a**) radial stress of the outer wall; (**b**) circumferential stress of the outer wall; (**c**) axial stress of the outer wall; (**d**) radial stress of the center; (**e**) circumferential stress of the center; (**f**) axial stress of the center; (**g**) radial stress of the inner wall; (**h**) circumferential stress of the inner wall; (**i**) axial stress of the inner wall.
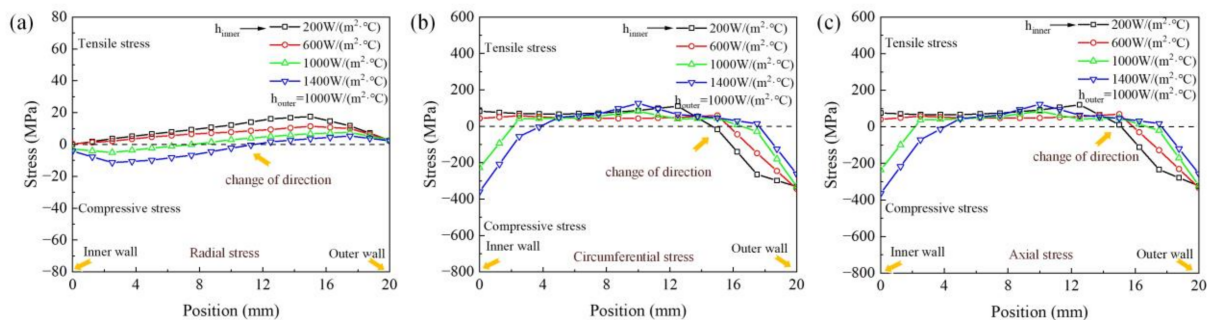
Figure 14. Stress distribution curve at different cooling intensities of the inner wall. (**a**) radial stress; (**b**) circumferential stress; (**c**) axial stress.

4. Conclusions

In this study, ANSYS simulation software was used to simulate the temperature and stress change of seamless steel tubes under different cooling intensities. By comparing the numerical simulation results of quenching residual stress of plate with the experimental data in reference [26], the accuracy of finite element simulation was verified. In addition,

the temperature and stress curves of the steel tube were obtained by changing the cooling intensity of the inner and outer walls. The main conclusions are as follows:

With the increase in the cooling intensity of the outer wall, the cooling rate increases gradually. The cooling rate of the center increases firstly and then decreases, and gradually approaches the cooling rate of the inner wall.

During the quenching process, the direction of the stress component will change. The cooling intensity of the inner and outer walls directly determines the stress size and distribution. Therefore, by controlling the cooling intensity of the inner and outer walls, the stress distribution position and stress state of the steel tube section can be controlled.

When the cooling intensity of the inner wall is less than that of the outer wall, the radial stress is tensile stress, the circumferential and axial stress near the outer wall is compressive stress, and the circumferential and axial stress near the inner wall is tensile stress. When the cooling intensity of the inner wall is equal to or greater than that of the outer wall, the radial stress near the inner wall is compressive stress, and the radial stress near the outer wall is tensile stress. The circumferential and axial stresses near the inner and outer walls are compressive stresses, and the central position is tensile stress.

The residual stress increases with the increase in the cooling intensity of the outer wall. The maximum stress is mainly concentrated on the near wall of the steel tube. With the increase in the cooling intensity of the inner wall, the residual stress firstly decreases and then increases. When the inner and outer wall cooling intensity is the same, the residual stress obtains a minimum value.

Author Contributions: Conceptualization writing—review and editing, Z.L.; investigation, writing—original draft preparation, R.Z.; software, D.C.; methodology, Q.X.; validation, J.K.; project administration, funding acquisition, G.Y.; supervision, G.W. All authors have read and agreed to the published version of the manuscript.

Institutional Review Board Statement: Not applicable.

Informed Consent Statement: Not applicable.

Data Availability Statement: Not applicable.

Conflicts of Interest: The authors declare no conflict of interest.

References

1. Chen, H.T.; Yan, R. Development progress and reflections of seamless tube industry in China. *Steel Roll* **2014**, *31*, 41–44.
2. Wang, H.H.; Sang, W.; Chen, J.D.; Chen, D. Summary of Domestic Development of Seamless Steel Tube of for Large-capacity Gas Cylinder Service. *Steel Tube* **2019**, *47*, 7–13.
3. Yuan, G.; Kang, J.; Li, Z.L.; Wang, G.D. Development of Technology for Microstructure Control during On-line Heat Treatment Process for Hot-rolled Seamless Steel Tube. *Steel Tube* **2018**, *47*, 30–34.
4. Chen, Z.; Chen, X.; Zhou, T. Microstructure and Mechanical Properties of J55 ERW Steel Tube Processed by On-Line Spray Water Cooling. *Metals* **2017**, *7*, 150. [CrossRef]
5. Liu, Y.; Zuo, X.-w.; Chen, N.-l.; Rong, Y.-h.; Liu, S.-j. Finite element simulation of longitudinal quenching crack. *Trans. Mater. Heat Treat.* **2019**, *40*, 160–167.
6. Zhao, Y.-F.; Liu, H.-S. Analysis of thermal stress in inhomogeneous long cylindrical superconductor. *J. Lanzhou Univ. Technol.* **2018**, *44*, 167–172.
7. Souza, J.L.F.; Ziviani, M.; Vitor, J.F.A. Mathematical modeling of tube cooling in a continuous bed. *Appl. Therm. Eng.* **2015**, *89*, 80–89. [CrossRef]
8. Raič, J.; Landfahrer, M.; Klarner, J.; Zmek, T.; Hochenauer, C. Modelling of the cooling process of steel tubes in a rake type cooling bed. *Appl. Therm. Eng.* **2020**, *169*, 114895. [CrossRef]
9. Raič, J.; Landfahrer, M.; Klarner, J.; Zmek, T.; Hochenauer, C. Coupled CFD simulation for the cooling process of steel tubes in a rake type cooling bed. *Appl. Therm. Eng.* **2020**, *171*, 115068. [CrossRef]

10. Chen, D.; Zhang, R.; Li, Y.; Li, Z.; Yuan, G. Online Cooling System and Improved Similar Self-adaptive Strategy for Hot-rolled Seamless Steel Tube. *ISIJ Int.* **2021**, *61*, 2135–2142. [CrossRef]

11. Mascarenhas, N.; Mudawar, I. Methodology for predicting spray quenching of thick-walled metal alloy tubes. *Int. J. Heat Mass Transf.* **2012**, *55*, 2953–2964. [CrossRef]

12. Ali, M.A.; Hasan, S.T.; Myriounis, D.P. A Method of Analysis to Estimate Thermal Down-Shock Stress Profiles in Hollow Cylinders when Subjected to Transient Heat/Cooling Cycle. In *Advanced Materials Research*; Trans Tech Publications, Ltd.: Freienbach, Switzerland, 2012; pp. 893–898.

13. Schemmel, M.; Prevedel, P.; Schöngrundner, R.; Ecker, W.; Antretter, T. Size Effects in Residual Stress Formation during Quenching of Cylinders Made of Hot-Work Tool Steel. *Adv. Mater. Sci. Eng.* **2015**, *2015*, 678056. [CrossRef]

14. Hata, T.; Sumi, N. Thermal stress-focusing effect in a cylinder with phase transformation. *Acta Mech.* **2008**, *195*, 69–80. [CrossRef]

15. De Oliveira, W.P.; Savi, M.A.; Pacheco, P.M.C.L.; de Souza, L.F.G. Thermomechanical analysis of steel cylinders quenching using a constitutive model with diffusional and non-diffusional phase transformations. *Mech. Mater.* **2010**, *42*, 31–43. [CrossRef]

16. Chen, X.; Zhang, K.; Chen, G.; Luo, G. Multiple axial cracks in a coated hollow cylinder due to thermal shock. *Int. J. Solids Struct.* **2006**, *43*, 6424–6435. [CrossRef]

17. Devynck, S.; Denis, S.; Bellot, J.P.; Bénard, T.; Gradeck, M. Influence of boiling heat transfer and phase transformations on the deformation of a steel tube during quenching by impinging water jets. *Materialwiss. Werkst.* **2016**, *47*, 755–761. [CrossRef]

18. Leitner, S.; Winter, G.; Klarner, J.; Antretter, T.; Ecker, W. Model-based Residual Stress Design in Multiphase Seamless Steel Tubes. *Materials* **2020**, *13*, 439. [CrossRef]

19. Yang, X.W.; Zhu, J.C.; Lai, Z.H.; Yong, L.I.U.; Dong, H.E.; Nong, Z.S. Finite element analysis of quenching temperature field, residual stress and distortion in A357 aluminum alloy large complicated thin-wall workpieces. *Trans. Nonferr. Met. Soc. China* **2013**, *23*, 1751–1760. [CrossRef]

20. Brunbauer, S.; Winter, G.; Antretter, T.; Staron, P.; Ecker, W. Residual stress and microstructure evolution in steel tubes for different cooling conditions—Simulation and verification. *Mat. Sci. Eng. A Struct.* **2019**, *747*, 73–79. [CrossRef]

21. Gao, J.N.; Gao, Y.; Xu, Q.R.; Wang, G.; Li, Q. Simulation on flow, heat transfer and stress characteristics of large-diameter thick-walled gas cylinders in quenching process under different water spray volumes. *J. Cent. South Univ.* **2020**, *26*, 3188–3199. [CrossRef]

22. Xie, J.B.; He, T.C.; Cheng, H.M. Study on the Thermal Stress Field of Steel 1045 Quenched by Water. *Adv. Mater. Res.* **2011**, *255*, 3568–3572. [CrossRef]

23. Wang, X.; Li, F.; Yang, Q.; He, A. FEM analysis for residual stress prediction in hot rolled steel strip during the run-out table cooling. *Appl. Math. Model.* **2013**, *37*, 586–609. [CrossRef]

24. Şimşir, C.; Gür, C.H. 3D FEM simulation of steel quenching and investigation of the effect of asymmetric geometry on residual stress distribution. *J. Mater. Process. Technol.* **2008**, *207*, 211–221. [CrossRef]

25. Gradeck, M.; Kouachi, A.; Lebouché, M.; Volle, F.; Maillet, D.; Borean, J.L. Boiling curves in relation to quenching of a high temperature moving surface with liquid jet impingement. *Int. J. Heat Mass Transf.* **2009**, *52*, 1094–1104. [CrossRef]

26. Koc, M.; Culp, J.; Altan, T. Prediction of residual stresses in quenched aluminum blocks and their reduction through cold working processes. *J. Mater. Process. Technol.* **2006**, *174*, 342–354. [CrossRef]